Biochemistry

pubs.acs.org/biochemistry Article

Mapping the Structural and Dynamic Determinants of pH-Sensitive Heparin Binding to Granulocyte Macrophage Colony Stimulating Factor

Jennifer Y. Cui, Fuming Zhang, Lukasz Nierzwicki, Giulia Palermo, Robert J. Linhardt, and George P. Lisi*

Cite This: *Biochemistry* 2020, 59, 3541−3553 Read Online

ABSTRACT: Granulocyte macrophage colony stimulating factor (GMCSF) is an immunomodulatory cytokine that is harnessed as a therapeutic. GMCSF is known to interact with other clinically important molecules, such as heparin, suggesting that endogenous and administered GMCSF has the potential to modulate orthogonal treatment outcomes. Thus, molecular level characterization of GMCSF and its interactions with biologically active compounds is critical to understanding these mechanisms and predicting clinical consequences. Here, we dissect the biophysical factors that facilitate the GMCSF−heparin interaction, previously shown to be pH-dependent, using nuclear magnetic resonance spectroscopy, surface plasmon resonance, and molecular dynamics simulations. We find that the affinity of GMCSF for heparin increases not only with a transition to acidic pH but also with an increase in heparin chain length. Changes in local flexibility, including a disruption of the N-terminal helix at acidic pH, also accompany the binding of heparin to GMCSF. We use molecular dynamics simulations to propose a mechanism in which a positive binding pocket that is not fully solvent accessible at neutral pH becomes more accessible at acidic pH, facilitating the binding of heparin to the protein.

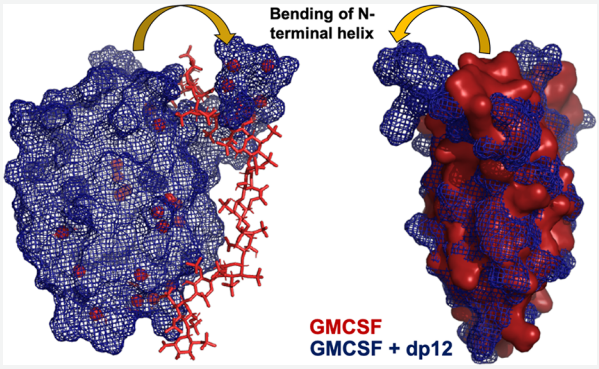

Granulocyte macrophage colony stimulating factor (GMCSF, or CSF2) is a mediator of cellular expansion and differentiation for myeloid progenitors in bone marrow. GMCSF plays an immunoregulatory role as a pathogenic pro-inflammatory agent in autoimmune diseases such as multiple sclerosis (MS) and rheumatoid arthritis (RA)[1,2] but has also been utilized in a clinical setting as a therapeutic for immunocompromised patients to simulate recovery of mature white blood cell populations.[3] Pathophysiological properties of GMCSF have been highlighted by the incidence of the global pandemic, COVID-19 (caused by SARS-CoV-2), where elevated levels of GMCSF were identified in COVID-19 patients in cases related to the development of systemic hyperinflammation, pneumonia, and acute respiratory distress syndrome (ARDS).[4] Attempts to mitigate hyperinflammatory conditions in these patients include development and testing of antibody-mediated therapeutics against GMCSF.[5−11] Given that GMCSF has been shown to be a protective and pathogenic signal transducer in innate immune responses, has been employed as a therapeutic for immunosuppressed patients, and is itself a drug target for COVID-19-related complications, insight into the mechanisms of GMCSF, particularly those involving molecules that modulate its structure, is of interest.[12] The interactions of GMCSF with several biologically relevant molecules, including heparin, heparan sulfate, chondroitin sulfates, and nucleotide triphosphates, have been investigated to various degrees at the biophysical level.[13−17] Heparin was previously reported to be an inhibitor of a nucleotide binding site that correlates directly to the proliferative ability of GMCSF, but the molecular details have not been established.[18] Exploring the mechanism of interaction between GMCSF and heparin will allow us to better understand how structural factors drive these and other protein−ligand interactions in this system.

Heparin functions endogenously as a cell surface glycosaminoglycan (GAG) and is clinically used as an anticoagulant. Unfractionated heparin, composed of a wide range of molecular weight oligosaccharides, is inexpensive and has well-characterized anticoagulative properties.[19,20] Low-molecular weight heparins, originally developed as alternatives to

Received: June 26, 2020
Revised: August 26, 2020
Published: September 8, 2020

https://dx.doi.org/10.1021/acs.biochem.0c00538
Biochemistry 2020, 59, 3541−3553

unfractionated heparin to reduce severe adverse immune reactions in a subset of patients, are now also routinely used in clinical applications ranging from dialysis to cardiac surgery.[21] However, recent reports have indicated that some patients testing positive for COVID-19 are experiencing higher than expected levels of stroke related to a hypercoagulative state, and COVID-19 patients that have stroke complications also have higher mortality rates.[22−24] Externally administered GMCSF was previously shown to induce mild activation of the coagulation cascade;[25,26] thus, it is even more critical to understand the GMCSF−heparin interaction at the molecular level to develop strategies for mitigating stroke complications in COVID-19 patients.

Prior work has shown that GMCSF can interact with heparin at acidic pH (pH 4−5) but does not interact at neutral pH.[13,16,17] The binding of GMCSF with negatively charged heparin molecules is reportedly dependent on three histidine residues (His15, His83, and His87) that become positively charged at acidic pH.[16] An additional residue, Lys85, is also thought to be involved. Interestingly, the clinical administration of GMCSF and heparin often occurs in patients experiencing pathologies with effects that alter the local physiological pH balance, such as asthma, sepsis, and cancer.[27−29] Given the frequent use of unfractionated and low-molecular weight heparin in clinical settings, and the role of GMCSF in altering immune responses, it is important to elucidate the interactions between these molecules, both of which exist endogenously and are administered as independent therapeutics, creating ample opportunity for them to exist in the same physiological space.

We explored the structural, dynamic, and biophysical properties of GMCSF−heparin complexes to better understand this interaction. Although a binding site for heparin on GMCSF has been proposed, there is no molecular level information about this interaction. Here, we use surface plasmon resonance (SPR) and solution nuclear magnetic resonance (NMR) to fill this knowledge gap by updating known binding interactions of unfractionated heparin with GMCSF, as well as providing novel probes of low-molecular weight heparin−GMCSF interactions. Additionally, we describe the biophysical changes in the GMCSF protein at acidic pH and in the presence of low-molecular weight heparins at neutral and acidic pH. Finally, we investigate the structure of GMCSF−heparin complexes with molecular dynamics (MD) simulations.

MATERIALS AND METHODS

Antibiotics used in protein expression and other analytical grade chemicals were purchased from Sigma. Unfractionated heparin was purchased from Sigma as a sodium salt. Heparin (16 kDa) and heparan sulfate (HS) (12 kDa) from porcine intestine were purchased from Celsus Laboratories (Cincinnati, OH). Heparin oligosaccharides, including the tetrasaccharide (dp4), hexasaccharide (dp6), octasaccharide (dp8), decasaccharide (dp10), and dodecasaccharide (dp12), were prepared from controlled partial heparin lyase 1 treatment of bovine lung heparin (Sigma) followed by size fractionation.

Protein Expression and Purification. Plasmid DNA containing GMCSF with an N-terminal six-His tag was cloned into a pET-15b vector and transformed into BL21(DE3) cells. GMCSF used in SPR experiments was grown and expressed in BL21(DE3) with LB medium at 37 °C. Isotopically enriched GMCSF was expressed at 37 °C in M9 minimal medium containing $CaCl_2$, $MgSO_4$, and MEM vitamins with $^{15}NH_4Cl$ as the sole nitrogen source. Small cultures of GMCSF were grown overnight in LB medium. The following morning, cloudy suspensions were collected by centrifugation and resuspended in the final M9 growth medium. Cultures of GMCSF were grown to an OD_{600} of 0.8−1.0 before induction with 1 mM isopropyl β-D-1-thiogalactopyranoside.

Cells were harvested after 5 h and resuspended in a denaturing lysis buffer containing 10 mM Tris-HCl, 100 mM sodium phosphate, and 6 M guanidine hydrochloride (GuHCl) at pH 8.0. Cells were lysed by sonication, and cell debris was removed by centrifugation. The resulting supernatant was incubated and nutated with 10 mL of Ni-NTA agarose beads for 30 min at room temperature before the Ni-NTA slurry was packed into a gravity column. The column was washed with the initial lysis buffer, followed by a gradient of the same buffer without GuHCl over 100 mL. Elution of GMCSF in its denatured form was performed with 1 column volume of a buffer containing 10 mM Tris-HCl, 100 mM sodium phosphate, and 250 mM imidazole (pH 8.0). GMCSF was refolded by dilution via dropwise addition of the 10 mL eluent into 100 mL of a refolding buffer containing 10 mM Tris-HCl, 100 mM sodium phosphate, and 750 mM arginine (pH 8.0). The refolded protein was dialyzed exhaustively against a buffer containing 2 mM sodium phosphate (pH 7.4). GMCSF was concentrated to ∼200 μM with an Amicon centrifugal device and stored at −20 °C.

Surface Plasmon Resonance. SPR measurements were performed on a BIAcore 3000 operated using BIAcore 3000 control and BIAevaluation software (version 4.0.1). Sensor SA chips were purchased from GE healthcare (Uppsala, Sweden).

Preparation of the Heparin Biochip. Biotinylated heparin was prepared by mixing 2 mg of heparin and 2 mg of amine−PEG3−Biotin (Thermo Scientific, Waltham, MA) with 10 mg of sodium cyanoborohydride ($NaCNBH_3$) in 200 μL of H_2O. The initial reaction was carried out at 70 °C for 24 h, after which an additional 10 mg of $NaCNBH_3$ was added to continue the reaction for an additional 24 h. The mixture was then desalted with a spin column (3000 molecular weight cutoff). Biotinylated heparin was freeze-dried for chip preparation. The biotinylated heparin was immobilized on a streptavidin (SA) chip based on the manufacturer's protocol. Briefly, a 20 μL solution of the heparin−biotin conjugate (0.1 mg/mL) in a buffer of 10 mM HEPES, 150 mM NaCl, 3 mM EDTA, and 0.005% surfactant P20 (pH 7.4) was injected over flow cell 2 (FC2), flow cell 3 (FC3), and flow cell 4 (FC4) of the SA chip at a flow rate of 10 μL/min. The successful immobilization of heparin was confirmed by the observation of an ∼100 resonance unit (RU) increase in the sensor chip signal. The control flow cell (FC1) was prepared by a 1 min injection with saturating biotin.

Measurement of Interaction between Heparin and GMCSF Using BIAcore. Samples of GMCSF were diluted in buffers containing 10 mM HEPES, 150 mM NaCl, 3 mM EDTA, and 0.005% surfactant P20 at pH 7.4, 5.5, and 4.5. Various dilute protein samples were injected at a flow rate of 30 μL/min. Following sample injection, the same buffer was passed over the sensor surface to facilitate dissociation. After dissociation for 3 min, the sensor surface was regenerated by injecting 30 μL of 0.25% sodium dodecyl sulfate (SDS). The response was monitored as a function of time (sensorgram) at 25 °C.

https://dx.doi.org/10.1021/acs.biochem.0c00538
Biochemistry 2020, 59, 3541−3553

Solution Competition Study between Heparin on the Chip Surface and Heparin-Derived Oligosaccharides in Solution. A heparin oligosaccharide competition study was carried out by mixing 1 μM GMCSF with 1 μM heparin oligos, including the tetrasaccharide (dp4), hexasaccharide (dp6), octasaccharide (dp8), decasaccharide (dp10), and dodecasaccharide (dp12), in 10 mM HEPES, 150 mM NaCl, 3 mM EDTA, and 0.005% surfactant P20 (pH 5.5). The mixtures were passed over the heparin chip at a rate of 30 μL/min. After each run, the dissociation and regeneration steps were performed as described above. For each set of competition experiments, a control experiment (GMCSF without any heparin or oligosaccharides) was performed to confirm complete regeneration of the chip surface and the reproducibility of results from multiple runs (n = 2 or 3). Steady-state dissociation constants for dissociation of heparin from GMCSF (k_d) were determined to occur outside of the time regime that could complicate interpretation of NMR experiments. Errors reported in Table 1 were determined as standard deviations from replicate experiments.

Table 1. pH-Dependent Binding Affinities of GMCSF for Heparin[a]

	k_a (M^{-1} s^{-1})	k_d (s^{-1})	K_D (M)
pH 7.4	63 ± 3	$4.2 \times 10^{-4} \pm 2.7 \times 10^{-5}$	6.8×10^{-6}
pH 5.5	68 ± 2	$3.9 \times 10^{-4} \pm 1.2 \times 10^{-5}$	5.8×10^{-6}
pH 4.5	2800 ± 90	$5.6 \times 10^{-4} \pm 2.0 \times 10^{-5}$	2.0×10^{-7}

[a]Sensorgrams of GMCSF−heparin interactions at pH 7.4, 5.5, and 4.5 show that the affinity of heparin for GMCSF increases with solution acidity, as shown by the reduction in K_D (Figure 1c, Table 1, and Figure S1), which was particularly pronounced as the pH changed from 5.5 to 4.5 and is primarily the result of the increased association rate (k_a) for association of heparin with GMCSF.

NMR Spectroscopy. NMR samples were prepared by dialyzing 200 μM GMCSF against a buffer of 20 mM HEPES and 1 mM EDTA at pH 7.4 or 5.5. NMR experiments were performed on a Bruker Avance NEO 600 MHz spectrometer at 20 °C. NMR data were processed in NMRPipe and analyzed in Sparky.[30,31] NMR assignments were initially determined with triple-resonance experiments at pH 7.4 and confirmed by BMRB entry 15531. Changes in resonance positions in GMCSF spectra at pH 5.5 were confirmed with standard triple-resonance experiments. The ^{1}H and ^{15}N carrier frequencies were set to the water resonance and 120 ppm, respectively. NMR titrations of heparins into GMCSF were performed by collecting a series of ^{1}H−^{15}N TROSY-HSQC spectra with an increasing heparin concentration until saturation was reached (i.e., no chemical shift perturbations were observed). Chemical shifts were evaluated separately at each pH to maintain consistency and eliminate the propagation of changes in NMR spectral data across different pH values. Trimmed means for chemical shift perturbation analyses were calculated by excluding the top and bottom 10% of the data sets (i.e., apo, +dp4, +dp12) collected at a given pH. Standard deviations were also determined from these data sets.

Longitudinal and transverse relaxation rates were determined from peak intensities of each amide resonance at multiple delay points after fitting to an exponential curve. Longitudinal and transverse relaxation rates were measured with relaxation times of 0, 20 (twice), 60 (twice), 100, 200, 600 (twice), 800, 1200, 1500, 2000, and 2500 ms for R_1 and 16.9, 33.9 (twice), 67.8, 136.0 (twice), 169.0, and 203.0 ms (twice) for R_2. Errors were determined from replicate spectra (n = 3 or 4). All relaxation experiments were carried out in a temperature-compensated interleaved manner, processed with in-house scripts, and analyzed in GraphPad Prism 7.0 (GraphPad Software). Trimmed means and standard deviations of relaxation data were determined as described above.

Molecular Dynamics Simulations. All simulations were based on the X-ray structure of GMCSF protein [Protein Data Bank (PDB) entry 2GMF].[32] Structures of heparin oligos were prepared using GLYCAM-Web GAG Builder.[33] Simulations were performed using the Gromacs 5 package[34] with the plumed 2.2 plugin.[35] The AMBER ff99SBnmr2 force field[36] was used for proteins, the GLYCAM-06j force field[37] for heparin, and the TIP3P model to represent water. In each simulated system, the numbers of Na^+ and Cl^- ions were adjusted to provide a physiological ionic strength (0.15 M). Simulations were carried out in the *NPT* ensemble with a temperature of 310 K with the v-rescale thermostat[38] and a pressure of 1 bar with the Parrinello−Rahman barostat.[39] Long-range electrostatic interactions were calculated with the particle mesh Ewald method[40] with a cutoff radius of 1 nm. van der Waals interactions were computed with a Lennard-Jones potential and a cutoff radius of 1 nm. All bonds involving hydrogen were restrained with the LINCS algorithm. The equations of motion were integrated with the leapfrog Verlet algorithm with a time step of 2 fs. Molecular images were created using VMD,[41] and plots were prepared using the matplotlib library.[42]

Spontaneous Binding of dp4 to GMCSF. The system was composed of single copies of GMCSF and dp4 embedded in a 7.1 nm × 7.1 nm × 7.1 nm dodecahedral box solvated with 7706 water molecules. To mimic the low-pH conditions, simulations were performed with His15, His83, and His87 protonated. To efficiently sample the possible states of binding of dp4 to GMCSF, the distance between centers of mass of portions of the protein backbone (residues 13−19, 83−87, and 118−122) and two or three sugar subunits of dp4 was restricted to 2.5 nm with one-sided harmonic potential with a spring constant of 500 kJ nm^{-2}. The system was simulated in six replicas, resulting in a 6 μs total sampling. The resulting trajectories were clustered on the basis of atomic positions of dp4 after superimposing the complex using backbone atoms of GMCSF residues 20−124 with cutoff of 0.3 nm via gmx cluster from the Gromacs package.

Refinement of GMCSF−dp12 Complexes. The system was composed of single copies of GMCSF and dp12 embedded in a 7.5 nm × 8 nm × 8 nm rectangular box solvated with 14961 water molecules. Similar to dp4 simulations, His15, His83, and His87 were kept in the protonated state. The intitial structure of GMCSF with dp12 was obtained by superimposing the dp12 molecule on the structure of the dp4−GMCSF complex in which dp4 formed direct contacts with His15, His83, and His87 residues. During the initial 10 ns equilibration of the complex, the root-mean-square deviation (RMSD)-based restraint was applied to the protein backbone region that initially interacted with dp4 (residues 4−15 and 82−87) with a force constant that gradually decreased from 4000 to 250 kJ nm^{-2}. At the same time, the orientation of the top four sugar subunits of dp12 was guided with RMSD-based restraints on a dp4−GMCSF structure from an initial value of 0.45 nm to a value of 0 nm

https://dx.doi.org/10.1021/acs.biochem.0c00538
Biochemistry 2020, 59, 3541−3553

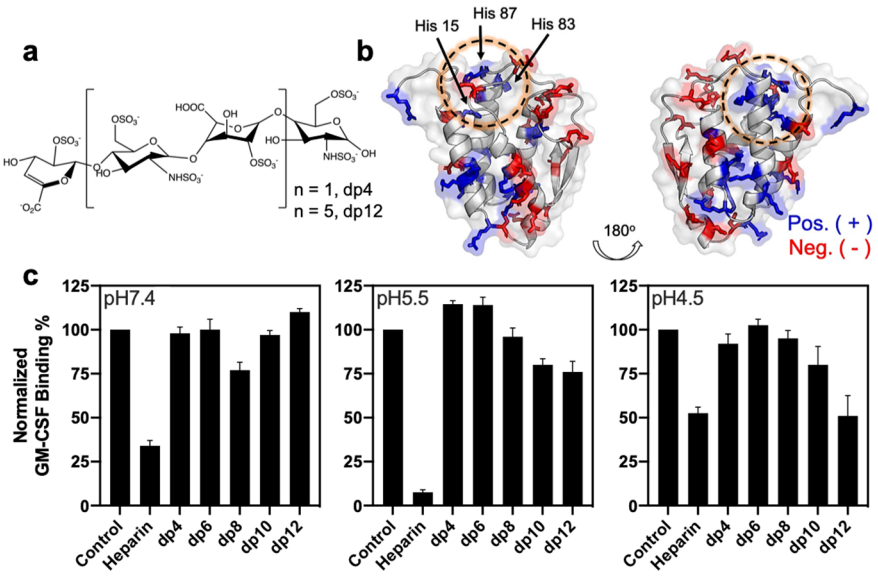

Figure 1. GMCSF−heparin interactions studied by SPR. (a) Structure of the major repeating sequence of heparin oligosaccharides (brackets) with degrees of polymerization (dp) of 4 and 12. (b) X-ray crystal structure of GMCSF (PDB entry 2GMF) showing the positively (Arg and Lys, blue) and negatively (Glu and Asp, red) charged residue distribution. The critical His residues clustered at the GMCSF termini are highlighted and circled. (c) Normalized competitive binding between immobilized heparin and aqueous solutions of GMCSF (1 μM, no competing ligand) and GMCSF complexed with unfractionated heparin (negative and positive controls) or heparin oligosaccharides dp4, dp6, dp8, dp10, and dp12 from SPR experiments conducted at pH 7.4, 5.5, and 4.5. Error bars were determined from replicate experiments.

with a force constant that gradually increased from 250 to 4000 kJ nm^{-2}. The system was additionally simulated for 10 ns with force constants for both restraints that gradually decreased to 0 kJ nm^{-2}. Finally, three replicas of conventional MD runs were performed for 1 μs each, and the trajectories were clustered according to the protocol described for the dp4−GMCSF complex.

Conventional Simulations of the GMCSF Protein. The systems were composed of single GMCSF proteins in a 7.1 nm × 7.1 nm × 7.1 nm dodecahedral box, filled with 7737 water molecules. GMCSF was simulated in two variants: with His15, His83, and His87 deprotonated, corresponding to a system at or above neutral pH, and with His15, His83, and His87 protonated, mimicking the protein at low pH. For each of the systems, we carried out 1 μs conventional MD runs. Residue-averaged root-mean-square fluctuations (RMSF) for each system were computed using gmx rmsf from the Gromacs package. The evolution of RMSF over time was computed in time intervals of ∼10 ns.

RESULTS

GMCSF−Heparin Interactions Are Size- and pH-Dependent. To assess the binding of unfractionated heparin and heparin oligosaccharides (oligos) to GMCSF (Figure 1), we used SPR. Sensorgrams collected with varying protein concentrations were globally fitted with a 1:1 Langmuir model, and the binding kinetics and affinities are listed in Table 1

We next performed solution/surface competition experiments in which preformed complexes of GMCSF and variably sized heparin oligos (Figure 1a, dp4, dp6, dp8, dp10, and dp12, where dp is the "degree of polymerization") were passed over a chip with immobilized heparin at pH 5.5 to examine the effect of heparin oligo chain size on the GMCSF−heparin interaction. Complexes of GMCSF and heparin oligos that had impaired binding to the chip surface were considered to have stronger binding interactions. GMCSF with heparin and GMCSF without heparin were used as controls. At pH 5.5, no competitive interaction was observed when 1 mM dp4, dp6, or dp8 was preincubated with GMCSF (Figure 1c). Indeed, it appears that dp4 and dp6 may even slightly enhance the binding of GMCSF to immobilized heparin, relative to that of the control sample. The extent of binding between surface-bound heparin and GMCSF was significantly diminished only in the presence of the dp10 and dp12 oligos, and 1 mM soluble heparin completely blocked binding. Similar experiments were conducted at pH 7.4 and 4.5 (Figure S1), suggesting that the interaction between GMCSF and heparin is pH-dependent and chain length-dependent beginning with a chain length of >8. On the basis of these data, we used dp4 and dp12 heparin oligos as representatives for each of the observed binding characteristics of heparin in subsequent biophysical experiments.

The GMCSF Structure and Molecular Motions Are Altered by Acidic pH. We obtained $^{1}H^{15}N$ heteronuclear single-quantum coherence (HSQC) NMR spectra of GMCSF at pH 7.4 and 5.5 to investigate the effect of acidic conditions, which favor heparin binding, on the GMCSF structure (Figures S2 and S3). We did not collect NMR data at pH 4.5, which crosses the isoelectric point of GMCSF, due to accelerated precipitation of the protein at NMR concentrations. Substantial chemical shift perturbations ($\Delta\delta$) are observed in the NMR spectrum of apo GMCSF at pH 5.5, highlighting changes in the local environments of residues primarily clustered around the histidine triad on helices A and C (residues 17−22 and 81−87, respectively), the loop connecting helix A and sheet β1 (residues 30−34), and the loop connecting sheet β1 and helix B [residues 47−55 (Figure 2a and Figure S4)].

Longitudinal (R_1) and transverse (R_2) relaxation rates measured by NMR highlight several regions of GMCSF with evidence of conformational flexibility (Figure 2b,c). Here, the pH-dependent relaxation rates are plotted as the R_1R_2 product

https://dx.doi.org/10.1021/acs.biochem.0c00538
Biochemistry 2020, 59, 3541−3553

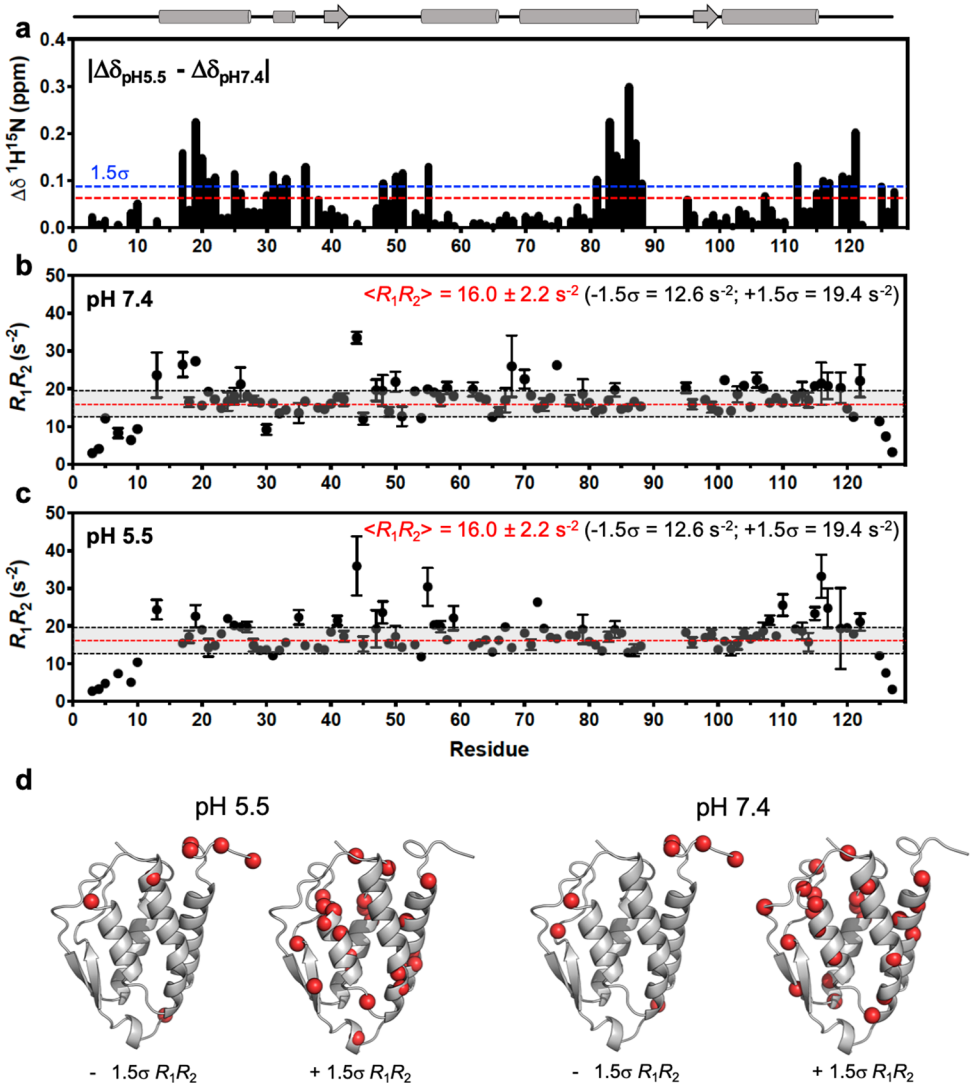

Figure 2. pH-dependent structural and dynamic changes in GMCSF. (a) Combined $^{1}H^{15}N$ chemical shift perturbations ($|\Delta\delta_{pH\ 5.5} - \Delta\delta_{pH\ 7.4}|$) calculated as $\Delta\delta = \sqrt{(\Delta\delta_{HN}{}^2 + \Delta\delta_{NH}{}^2/25)/2}$. The red and blue lines denote the 10% trimmed mean of the data and 1.5σ above the mean, respectively. A cartoon representation of the GMCSF structure is shown above the panel. (b) NMR R_1R_2 relaxation parameters for apo GMCSF at pH 7.4. The red dashed line denotes the 10% trimmed mean of all relaxation data, and the gray shaded area denotes ±1.5σ. The 10% trimmed mean and ±1.5σ values are also listed. (c) NMR R_1R_2 relaxation parameters for apo GMCSF at pH 5.5. The red dashed line again denotes the 10% trimmed mean of all relaxation data, and the gray shaded area denotes ±1.5σ. (d) Residues with R_1R_2 values below (−1.5σ) or above (1.5σ) the 10% trimmed mean R_1R_2 are mapped onto the GMCSF structure (PDB entry 2GMF). Tables S1−S4 list all R_1R_2 rates for residues mapped on the GMCSF structure. Residues with R_1R_2 values outside the ±1.5σ boundaries but error bars within the ±1.5σ boundaries are also depicted on these structures.

to suppress contributions of anisotropic molecular tumbling that complicate interpretations of chemical exchange.[43] Average R_1R_2 values for each pH condition were 16.38 ± 0.54 s^{-2} (pH 5.5) and 15.65 ± 1.3 s^{-2} (pH 7.4), and the average R_1R_2 determined from collective analysis of all relaxation data was 16.0 ± 2.2 s^{-2}, which is plotted as a measure of statistical significance.[44,45] The average generalized order parameter was estimated with the equation $S_{avg}{}^2 = \sqrt{R_1R_2/R_1R_2^{max}}$, using values of $\langle R_1R_2\rangle$ and $R_1R_2^{max}$ that reflect the entire data sets.[43] At neutral pH, seven residues within the core of GMCSF [N17, I19, S44, L70, G75, I101, and F106 (Figure 2d)] display R_1R_2 values above 1.5σ of the 10% trimmed mean of all measured rates, possibly due to the influence of R_{ex} related to microsecond to millisecond motion. An additional eight residues show R_1R_2 values well below 1.5σ of the 10% trimmed mean, qualitatively suggesting picosecond to nanosecond time scale motion, as the average order parameter of the protein estimated from the entire data set (S^2) is 0.69. A majority of residues with depressed R_1R_2 values are found at the N- and C-termini, proximal to the histidine triad, while R30 and E45 are within loops or unstructured regions of the protein (Figure S5). At acidic pH, more microsecond-to-millisecond motions may be present within the protein core and one face of the protein, based on regions along helices A, C, and D that have a greater number of R_1R_2 values substantially elevated above 1.5σ of the 10% trimmed mean, including W13, I19, R24, E35, S44, D48, L55, K72, L110, L115, and V116 (Figure 2d, Figure S5, and Table S1). Regions suggestive of fast time scale dynamics are practically unchanged, restricted to terminal residues [namely N-terminal

https://dx.doi.org/10.1021/acs.biochem.0c00538
Biochemistry 2020, 59, 3541−3553

A3, R4, S5, S7, S9, and T10 (Table S1)] showing an average generalized order parameter across GMCSF (S^2) of 0.68 at pH 5.5, essentially within error of S^2 estimated at pH 7.4.

The Structure and Dynamics of GMCSF Are Altered in a pH- and Heparin Size-Dependent Manner. ^{15}N-labeled GMCSF was titrated with unfractionated heparin (containing low- and high-molecular weight species), dp4, and dp12 at pH 7.4 and 5.5, to further characterize heparin binding. Combined $^{1}H^{15}N$ HSQC spectral perturbations were analyzed separately in each pH regime to capture the effects of heparin oligos without propagating the "baseline" effect of pH on apo GMCSF reported in Figure 2a. At pH 7.4, unfractionated heparin did not cause any chemical shift perturbations in the GMCSF NMR spectrum (Figure 3a). Similarly, titration of

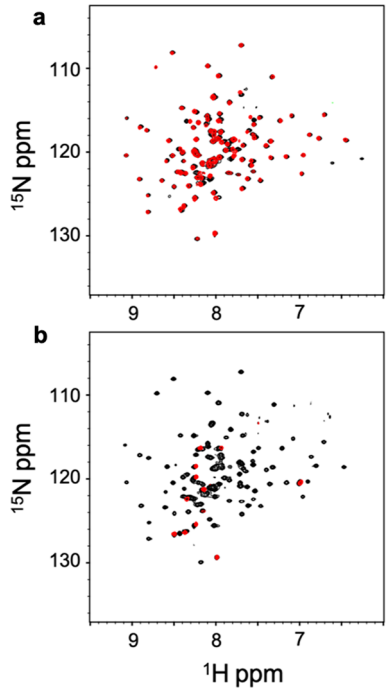

Figure 3. pH-dependent interaction of GMCSF with unfractionated heparin. (a) $^{1}H^{15}N$ HSQC NMR spectrum of GMCSF at pH 7.4 (black) and GMCSF saturated with unfractionated heparin (red). (b) Spectrum from an identical experiment carried out at pH 5.5.

GMCSF with dp4 at pH 7.4 perturbs only two resonances, corresponding to E14 and L55 on helices A and B (Figure 4a and Figures S2a and S4). However, when dp12 is titrated into GMCSF at pH 7.4, chemical shifts of 27 residues are perturbed (Figure 4a and Figure S2b).

The NMR spectrum of apo GMCSF at pH 5.5 was altered more substantially by heparin oligos, in a manner distinct from that of the acidic pH itself (Figure 2a and Figure S3). In the presence of unfractionated heparin at pH 5.5, the entire NMR spectrum of GMCSF is broadened beyond detection, with the exception of 10 N- and C-terminal resonances (Figure 3b). Presumably, this is due to the formation of a large complex with slow molecular tumbling that has been previously reported in other work.[17] Titration of GMCSF with dp4 at pH 5.5 revealed 10 strongly perturbed chemical shifts, and a much greater level of overall perturbation relative to its apo reference spectrum (Figure 4b and Figure S2c). Five resonances were also broadened beyond detection but were not localized to any specific region within GMCSF (Figures S5 and S6 and Table S2). Although the binding of dp12 to GMCSF at pH 5.5 induced chemical shift perturbations in only 13 resonances, these shifts were quite strong, and an additional 16 resonances were broadened beyond detection, suggesting a change in the conformational exchange regime of these sites (Figure 4b and Figure S2d). Interestingly, a majority of these line-broadened residues were clustered directly around the histidine triad believed to be critical for heparin binding, most notably residues 17−21 along the positively charged α-helical face of GMCSF (Figures S5 and S6 and Table S2). Overall, dp12, the strongest binder of GMCSF in SPR experiments, caused the greatest number and magnitude of chemical shift perturbations at both neutral and acidic pH (Figure 4 and Figure S3). The results of these NMR titrations are mapped onto the GMCSF structure in Figure 5, showing 21 residues (including those line-broadened beyond detection) affected by dp12 in nearly identical locations.

Binding of Heparin to GMCSF Modulates Protein Motions. At neutral pH, values of the R_1R_2 product determined with NMR spin relaxation experiments on the GMCSF−dp4 complex do not differ that substantially from those of apo GMCSF [$\langle R_1R_2\rangle_{apo}$ = 16.93 s^{-2}; $\langle R_1R_2\rangle_{dp4}$ = 16.38 s^{-2} (Table S4)], with the exception of residues showing a depressed R_1R_2 (-1.5σ) in the GMCSF−dp4 complex, localized along the surface of the protein surrounding the N- and C-termini as well as the positively charged helix A (Figure S5b). Sites with elevated ($+1.5\sigma$) R_1R_2 parameters in apo GMCSF are diminished, perhaps due to stabilization of GMCSF from dp4 binding, at pH 7.4. Saturation of GMSCF with dp12 restores apo-like R_1R_2 readouts, including weakly at residues 24−28 adjacent to the histidine triad, and more substantially at several sites thoughout the protein core, suggestive of microsecond-to-millisecond motion (Figure S5c and Table S3). Regions of apparent flexibility in apo GMCSF and its complexes with dp4 and dp12 differ only locally in these samples (Figure S5 and Tables S1−S3), and we speculate that subtle modulation of the dynamics in residues surrounding the supposed histidine binding site or terminal helices could play a role in heparin docking, based on the varied impact of heparins on GMCSF NMR spectra.

When dp4 was titrated into GMCSF at pH 5.5, protein motions on the microsecond-to-millisecond ($+1.5\sigma$) and picosecond-to-nanosecond (-1.5σ) time scales are suggested, including at many sites distinct from apo GMCSF [encompassing $\pm1.5\sigma$ (Tables S1 and S2)]. Evidence of flexibility clustered around the N-terminus (residues 3−10), the linker region between helices A and β1 (residues 30−49), and some residues within helix C (composed of residues 65−88) is observed (Figure S5 and Table S2). Five additional residues are line-broadened beyond detection (Figure S6), a classical signature of millisecond dynamics[46] that is neither observed in the identical experiment at pH 7.4 nor caused solely by a change in pH. When GMCSF is titrated with dp12 at pH 5.5, 11 residues show R_1R_2 values $\geq1.5\sigma$ of the 10% trimmed mean [most prominently S44, L59, L70, V116, and F119 (Table S3)], while 16 additional resonances are broadened beyond detection (Figure 6b, Figure S6, and Table S3), also suggestive of millisecond motion. In the GMCSF−dp12 complex, line-broadened residues are localized directly along the N-terminal α-helix and surface-exposed areas of adjacent helices, highlighting the unique effect of larger heparin oligos on the acidic form of GMCSF and its purported binding site. Severe line broadening, which precludes

https://dx.doi.org/10.1021/acs.biochem.0c00538
Biochemistry 2020, 59, 3541−3553

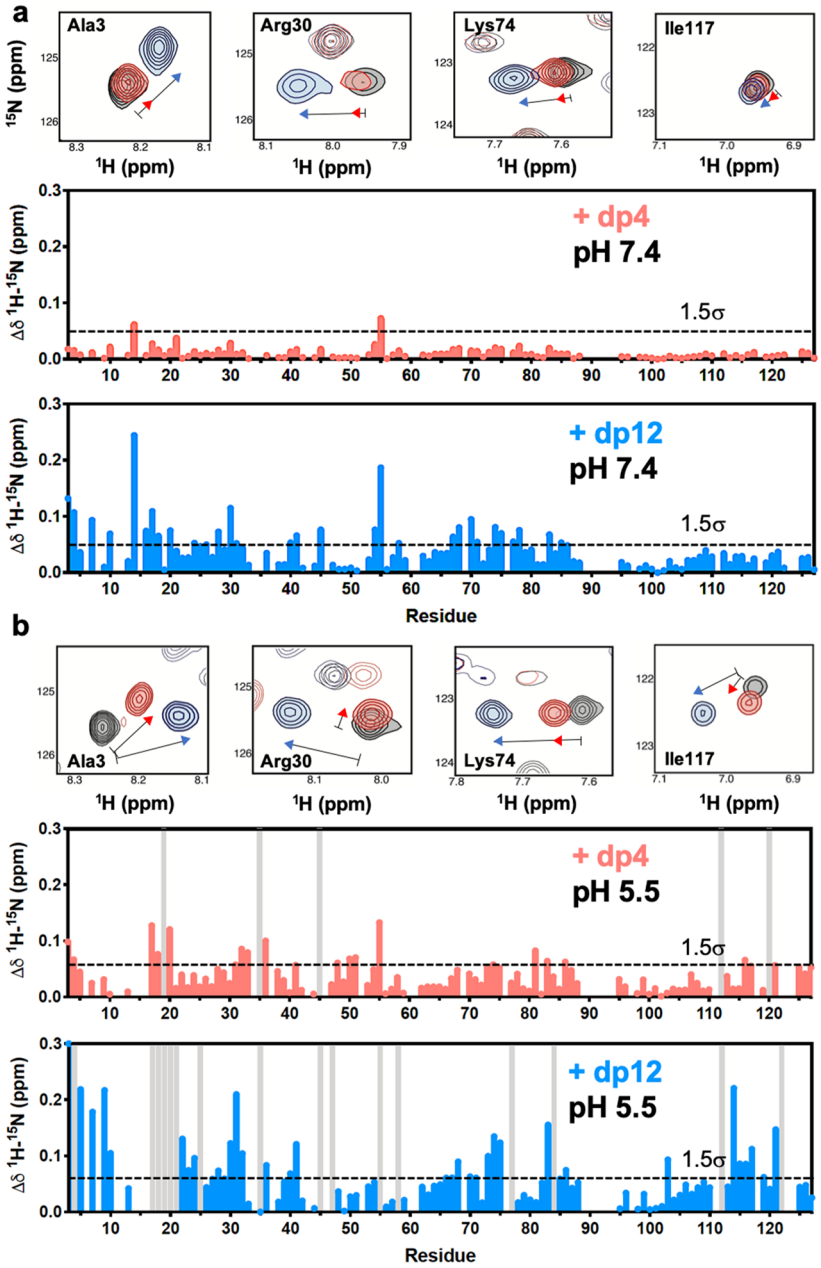

Figure 4. Heparin-dependent structural changes in GMCSF. (a) Combined $^{1}H^{15}N$ chemical shift perturbations caused by binding of dp4 (red) and dp12 (blue) to GMSCF at pH 7.4. Selected NMR resonances are shown to illustrate differences in chemical shift behavior of apo GMCSF (black resonances) in the presence of dp4 (red) and dp12 (blue). (b) Combined $^{1}H^{15}N$ chemical shift perturbations caused by binding of dp4 (red) and dp12 (blue) to GMSCF at pH 5.5. NMR resonances again illustrate differences in chemical shift behavior of apo GMCSF (black) in the presence of dp4 (red) and dp12 (blue). Combined chemical shift perturbations in panels a and b were calculated with the equation $\Delta\delta = \sqrt{(\Delta\delta_{HN}{}^{2} + \Delta\delta_{NH}{}^{2}/25)/2}$. Dashed lines represent 1.5σ above the 10% trimmed mean of all shifts measured at each pH value and are used as a significance cutoff. Gray bars indicate instances in which the resonance was broadened beyond detection.

relaxation analysis, is depicted with gray bars in Figure 6. The disappearance of these resonances from the dp12-bound NMR spectrum is also highlighted in Figure S6.

To ensure that NMR-detected dynamics were not due to equilibrium fluctuations caused by heparin binding and/or unbinding, we performed NMR line shape analysis. The average k_{off} determined from line shape fitting of one-dimensional slices of $^{1}H-^{15}N$ correlation spectra is $(2.2 \pm 0.3) \times 10^{-1}$ s^{-1} (Figure S7), suggesting the time scale for this process occurs outside the exchange regime probed by NMR spin relaxation, where typical k_{ex} values range from 100 to 3000 s^{-1}.[46] Variations in k_{off} from fits of the ^{1}H versus ^{15}N dimensions (Figure S7) may arise from asymmetry in the chemical shift trajectory, which often exhibits stronger shifts in one dimension that are easier to fit, or from standard errors associated with the fitting algorithms.[47] Nonetheless, fitted rates are outside the microsecond-to-millisecond k_{ex} regime, as are k_{off} values derived from SPR (Table 1). Differences in the SPR and NMR techniques themselves, which have been noted several times in the literature,[48−50] likely account for some variance in the calculated k_{off} parameters. Overall, the dynamic character of apo GMCSF is fairly similar at pH 7.4 and 5.5,

https://dx.doi.org/10.1021/acs.biochem.0c00538
Biochemistry 2020, 59, 3541−3553

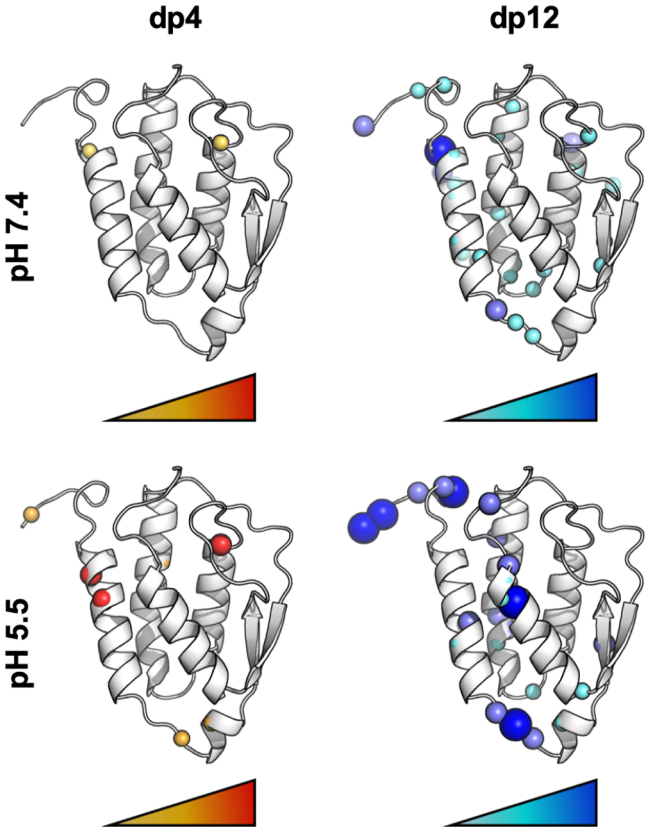

Figure 5. pH- and heparin size-dependent structural changes in GMCSF. Chemical shift perturbations $\geq 1.5\sigma$ above the 10% trimmed mean of data collected at pH 7.4 (top) and pH 5.5 (bottom) plotted on the GMCSF structure. Spheres are sized and colored with increasing magnitude of chemical shift (dp4, yellow → red; dp12, cyan → dark blue).

with the acidic form showing slightly more flexibility at the termini surrounding the histidine triad. Binding of heparin oligos to GMCSF activates different patches of residues as a function of pH and oligo size (Figures S5, S8, and S9 and Tables S1−S3). The most striking difference among these complexes is the degree of NMR line broadening observed exclusively at pH 5.5.

In an attempt to visualize how similar (or different) R_1R_2 relaxation parameters of dp4- and dp12-bound GMCSF were to those of apo GMCSF, we conducted a correlation analysis between these samples, where no change in R_1R_2 values across the protein sequence would be expected to produce a linear relationship (Figures S8 and S9). This comparison revealed a greater deviation from linearity in heparin-bound GMCSF complexes at pH 5.5 (Figures S8 and S9), suggesting that overall, subtle differences in GMCSF dynamics influenced by oligo size were most different from those of the apoprotein at acidic pH (Figures S8 and S9). Heparin size-dependent differences in our NMR chemical shift and relaxation data suggest that the length of the saccharide chain affects its mode of interaction with GMCSF. Likewise, heparin-bound GMCSF complexes showed greater variability in relaxation parameters relative to each other (i.e., dp4 vs dp12) at acidic pH.

Molecular Dynamics Simulations Establish Structural Models for GMCSF−Heparin Complexes. Finally, to evaluate possible GMCSF−heparin structures at low pH, we performed MD simulations in six replicas of 1 μs each for the spontaneous binding of dp4 to GMCSF. Next, we clustered the trajectories according to the positioning of dp4 with respect to GMCSF. This approach led us to identify two major binding poses (Figure 7a), which contributes to ∼50% of the total trajectory length. In these binding poses, dp4 either enters a binding pocket formed by His15, His83, and His87 or docks at the positive interface of GMCSF helices A and C (Figures 1b and 7a and Figure S4). Notably, both of these binding poses are located in the immediate proximity of each other, suggesting that a similar binding region may be shared by longer heparin oligos. To verify this hypothesis, we performed additional MD simulations in three replicas with a total length of 3 μs of dp12 initially docked to the binding pocket of GMCSF formed by His15, His83, and His87. As revealed by cluster analysis, dp12 rapidly fits in a cavity between helices A and C of GMCSF during simulations, forming a well-defined complex (Figure 7b and Figure S10), in very good agreement with NMR perturbations of GMCSF upon dp12 binding (Figure 4), as well as with heparin-specific molecular docking algorithms (Figure S11).

To understand how acidic pH and heparin binding perturb the GMCSF structure, we performed two additional MD runs of 1 μs each of GMCSF with histidine residues forming the binding pocket in protonated or deprotonated forms. Next, we computed the residue-averaged RMSF and the evolution of RMSF over time for GMCSF in each simulated system. This analysis shows that at higher pH values, where histidine residues are deprotonated, structural fluctuations of the GMCSF protein are generally low (Figure 7c and Figure S12). Protonation of histidine residues leads to an increased number of fluctuations at the N-terminal portion of GMCSF. Beyond the N-terminus, a strong dynamic feature is observed in dp4-bound GMCSF at pH 5.5 (Figure 7c). Analysis of pH-dependent NMR relaxation rates shows that at pH 5.5, dp4 most strongly alters R_1R_2 parameters at the GMCSF termini and within the protein core spanning residues 50−75 (Figure S9b). Larger fluctuations of the protonated GMCSF structure suggest increased dynamics in backbone N−H bond vectors on the picosecond-to-nanosecond time scale, which is consistent with NMR data showing depressed R_1R_2 parameters surrounding the histidine triad, and may also explain smaller average R_1R_2 values for heparin-bound GMCSF complexes (Table S4). These fluctuations are further magnified by binding of heparin oligos, particularly dp12, where multiple events corresponding to the high RMSF of the N-terminal loop occur over ∼700 ns (Figure S12). These findings are consistent with NMR ΔR_1R_2 plots that show heparin-induced changes to relaxation parameters at the N- and C-termini of GMCSF (Figure S8c), which are less apparent at neutral pH (Figure S8d). Overall, MD simulations suggest that the increased dynamics of the N-terminus of GMCSF might facilitate heparin binding, while NMR shows that although the global effect of dp4 and dp12 is fairly consistent across the protein, local differences corresponding to terminal regions and sites observed during MD simulations may contribute to complex formation.

DISCUSSION

GMCSF is an important mediator of innate immunity and was previously shown to form pH-dependent complexes with heparin using analytical and affinity chromatography and light scattering.[13,16,17] The electrostatic interaction between GMCSF and heparin is proposed to be predominantly

https://dx.doi.org/10.1021/acs.biochem.0c00538
Biochemistry 2020, 59, 3541−3553

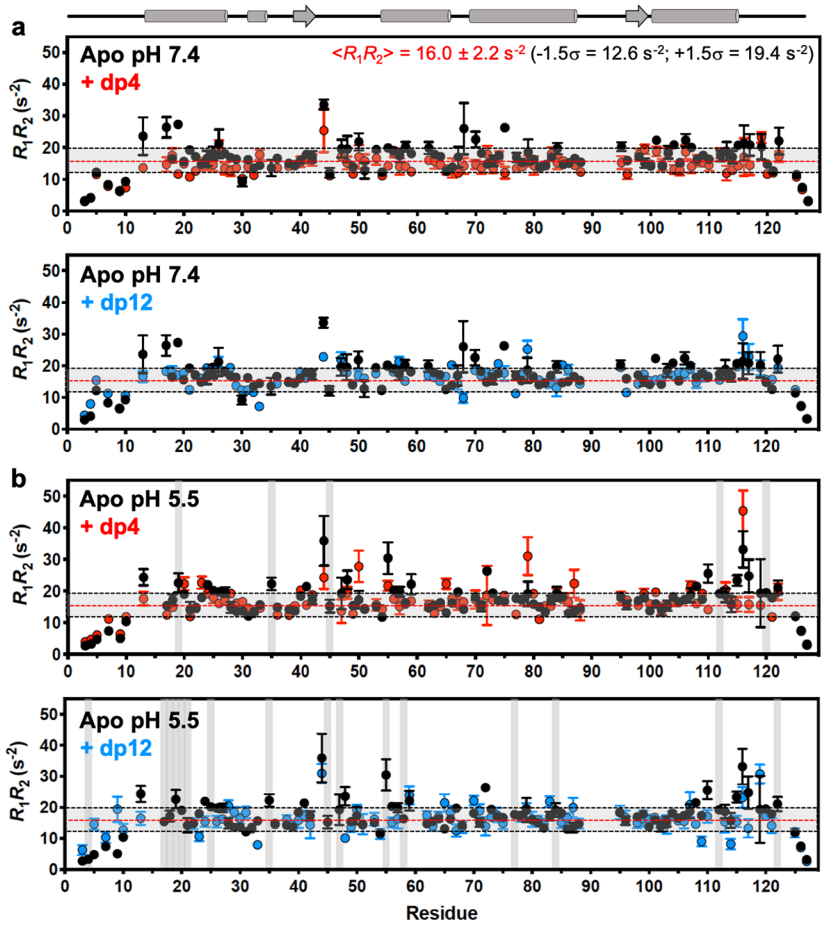

Figure 6. Dynamics of GMCSF−heparin complexes. (a) Plots of R_1R_2 relaxation parameters determined by NMR for apo GMCSF (black circles) and in the presence of dp4 (red circles) or dp12 (blue circles) at pH 7.4. Gray shaded areas mark $\pm 1.5\sigma$ from the 10% trimmed mean (red line) of all relaxation rates. The 10% trimmed mean and $\pm 1.5\sigma$ values are also listed. A cartoon representation of the GMCSF structure is shown above the panel. (b) Identical plots showing the heparin size dependence of R_1R_2 relaxation parameters at pH 5.5 for apo GMCSF (black) and in the presence of dp4 (red) or dp12 (blue). Gray shaded areas mark $\pm 1.5\sigma$ from the 10% trimmed mean (red line) of all relaxation rates. Vertical gray bars represent instances of line broadening in the NMR spectrum of heparin-saturated GMCSF. Numerical summaries of these plots are listed in Tables S1−S3.

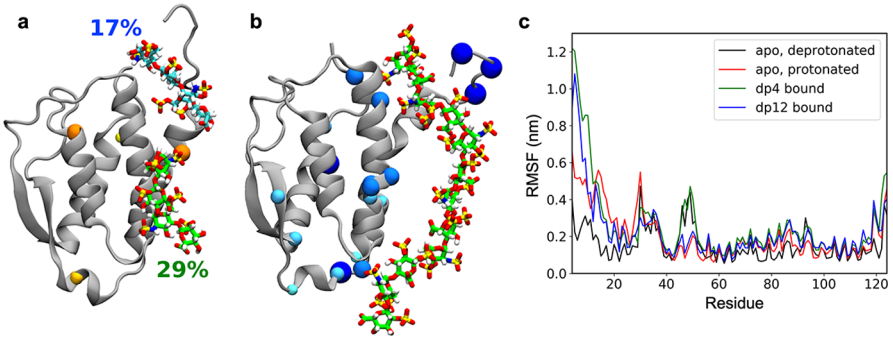

Figure 7. MD simulations of GMCSF−heparin complexes. (a) Cluster analysis of the two main complexes of dp4 with GMCSF. These poses account for ∼50% of the total simulation time (percentages of total simulation time are indicated next to each structure). A separation of the N-terminal helix from the protein core is observed. Spheres are sized and colored with the increasing magnitude of the NMR chemical shift (yellow → orange). (b) Cluster analysis of the major GMCSF−dp12 complex, bound at the His_3 site, where a significant bend in the N-terminal helix exposes the His residues. Spheres are sized and colored with the increasing magnitude of the NMR chemical shift (cyan → dark blue). (c) RMSFs of apo GMCSF at neutral (black) and acidic (red) pH, and at acidic pH bound to dp4 (green) and dp12 (blue). RMSFs at the N-terminus of GMCSF and along the positive interface (residues 40−60) are much larger in the presence of heparin oligos (black vs blue; black vs green) than those caused by a change in pH alone (black vs red), indicating a specific effect of the heparin oligos.

mediated by histidine residues (His15, His83, and His87) that ionize at acidic pH. These residues form a positively charged binding pocket for heparin, which is abrogated upon mutation of these His residues.[16] However, the structural changes associated with the binding of heparin to GMCSF are not well-defined. We used SPR, NMR, and MD simulations to dissect

https://dx.doi.org/10.1021/acs.biochem.0c00538
Biochemistry 2020, 59, 3541−3553

the GMCSF−heparin interaction at the molecular level. SPR sensorgrams confirm that heparin binds to GMCSF in a pH-dependent manner. The rate of association of heparin with GMCSF increases (i.e., tighter binding) at pH 4.5, and the binding affinity of heparin for GMCSF increases from 6.75×10^{-6} to 1.99×10^{-7} M over the pH range studied (7.4−4.5). These data are consistent with a GMCSF binding pocket that is optimized for heparin at acidic pH. Interestingly, SPR data suggest that GMCSF and heparin interact at neutral pH, as well, albeit with an affinity that is approximately 1 order of magnitude lower, which has never been reported. It is possible that this interaction is transient and cannot be easily detected with the biochemical assays used in previous work. Indeed, titration of heparin into GMCSF at neutral pH monitored by NMR, which readily detects both transient and tightly bound complexes,[46] showed chemical shift perturbations consistent with an interaction.

Although it was previously reported that the molecular weight of heparin did not affect its interactions with GMCSF,[13] we found the GMCSF−heparin interaction to be oligo size-dependent (Figures 1c and 3). The lack of a previously observed size dependence may be attributed to the use of heterogeneous, polydisperse low-molecular weight heparins, which have repeating heparin disaccharide units ranging from dp4 to larger than dp24. In contrast, we found that the critical size for a difference in binding character in a homogeneous population is larger than dp8. On first examination, it appears that GMCSF−heparin complexes with dp values of ≥10 diminish sequestration of GMCSF by immobilized heparin (Figure 1c); thus, GMCSF efficiently binds only heparins of a minimum size threshold (larger than dp8). This is also reflected in the number of residues that undergo chemical shift perturbations during NMR titrations of GMCSF with dp4 at pH 5.5, which is significantly reduced from that of the identical experiment with dp12 (Figures 2 and 4). However, a closer examination of SPR data suggests that dp4 can increase the efficiency by which GMCSF and immobilized heparin interact compared to that of GMCSF alone.

We recorded $^{1}H^{15}N$ HSQC spectra of apo GMCSF and apo GMCSF with saturating amounts of unfractionated heparin, dp4, and dp12 at pH 7.4 and 5.5 and found that unfractionated heparin did not cause any chemical shift perturbations at pH 7.4. However, when the experiment was repeated at pH 5.5, the HSQC spectrum was almost entirely broadened beyond detection, suggesting formation of a much larger complex that limits the ability of GMCSF to tumble efficiently in solution. The average molecular weight of a heparin chain in an unfractionated mixture is ∼15 kDa (nearly the size of GMCSF); thus, aggregates were expected and posed a technical challenge in that the resulting molecule appeared to be too large for the NMR study, precluding useful structural information about GMCSF−heparin complexes. We therefore used biosynthesized heparin oligos at shorter chain lengths so that if complexes were formed with GMCSF, they would remain small enough to maintain resolution by NMR and circumvent this problem.

Solution NMR experiments indicate GMCSF experiences unique local changes in structure and dynamics at neutral and acidic pH, consistent with previously reported differences in light scattering characteristics of GMCSF at pH 7.0 and 4.0.[17] NMR experiments indicate that apo GMCSF displays similar molecular motions in residues within or proximal to the heparin docking site at pH 7.4 and 5.5 (Figure S9). In contrast, the R_1R_2 profiles of heparin-bound GMCSF are subtly altered in various regions of the protein, perhaps due to the heparin oligo (de)stabilizing nearby structural elements through binding, which in turn propagate to amino acids in adjacent helices.

It is possible that altered backbone dynamics in the acidic form of GMCSF may allow heparin to access the N-terminal His residues to form stronger contacts (Figure 7). However, a greater overall positive charge of the GMCSF protein could also produce this effect. NMR chemical shifts caused by a change from pH 7.4 to 5.5 are consistent with local structural alterations, and heparin-induced NMR chemical shift perturbations are stronger at acidic pH (Figure 4) and also show severe line broadening, again hinting at contributions from optimized electrostatics and dynamics, respectively. However, questions of dynamic versus electrostatic contribution are likely to be complicated in solution, and subsequent mutagenesis studies will be conducted to provide further insight into the molecular role of these phenomena.

Novel MD simulations shed some light, as they demonstrate that a change in pH alone does not induce the same degree of large RMSF caused by heparin binding (Figure 7), suggesting that GMCSF alone becomes dynamic at pH 5.5, and heparins more strongly alter this state. These data are consistent with NMR results showing changes in the specific residues undergoing fluctuations (Figures S5, S8, and S9 and Tables S1−S3), as well as with NMR line broadening observed at only pH 5.5 in the presence of heparin oligos (Figure S6). Strikingly, MD simulations also show that heparin binding bends the terminal helices of the protein away from the core, facilitating the His−heparin interaction at pH 5.5. Again, understanding the extent that repulsion of ionized His residues could drive this process before heparin binding, as opposed to structural dynamics simply allowing GMCSF to sample this altered conformation in the presence of heparins, requires further investigation.

Light scattering and sedimentation results of Wettreich and co-workers previously suggested that for large GMCSF−GAG complexes to form, multiple points of contact for heparin on GMCSF must exist.[17] However, a second binding surface was not conclusively identified. Our combined SPR and NMR data suggest that GMCSF has a preferential binding site, likely mediated by strong electrostatic interactions suggested in prior work. The second binding interaction is likely made available upon the first GMCSF−heparin contact and is dependent on heparin chain length. The primary mediators of GMCSF−heparin interactions were previously reported to be His15, His83, and His87, though these histidine residues are not fully solvent exposed in the GMCSF crystal structure. However, we speculated that the heightened flexibility of the GMCSF termini could destabilize noncovalent interactions between these π-stacked histidine residues and that molecular motions could optimize the positively charged histidine binding pocket for negatively charged heparin. Indeed, MD simulations carried out on dp4− and dp12−GMCSF complexes demonstrate that dp4 forms interactions with this positively charged cleft or the adjacent positive residues along the N-terminal face of GMCSF in a manner consistent with NMR chemical shift perturbations (Figure 7). MD simulations also show that larger oligos can further interface along helices A and C, where there is another cluster of positively charged residues. These helices showed evidence of flexibility in NMR relaxation experiments (Figures 2 and 6 and Figure S5) and are the sites of significant

https://dx.doi.org/10.1021/acs.biochem.0c00538
Biochemistry 2020, 59, 3541−3553

chemical shift perturbations during dp12 titrations (Figure 4). These chemical shift signatures are exclusive to dp12, consistent with shorter heparin oligos simply not being large enough to dock with this region of GMCSF. Our model of the GMCSF−heparin structure is further supported by the docking of heparins onto GMCSF with a heparin-specific algorithm that accounts for shallow charged pockets optimized for polysaccharides within ClusPro (Figure S11). Consistent with NMR chemical shifts and MD, all docked poses occur on the positively charged face of GMCSF.

Backbone RMSFs determined from MD suggest that acidic pH modulates the fluctuations of apo GMCSF as well as its heparin-bound complexes. These changes in local flexibility, also observed by NMR, may contribute to the higher affinity of heparins for GMCSF at pH ≤5.5. MD simulations show that dp4 and dp12 oligos bend the N-terminal helix away from the protein core (Figure 7), implying a mechanism in which protein motions of GMCSF weaken intramolecular forces to allow heparin oligos to access the binding pocket. Although the largest NMR chemical shift perturbations are observed along the heparin binding face of GMCSF, it should be noted that chemical shift perturbations are also observed beyond the heparin docking sites, indicating that heparins either propagate a binding signal to distal regions of GMCSF (potentially by altering the position of the N-terminal helix) or interact transiently with other portions of the protein. A follow-up study utilizing point mutations at the critical His residues will ultimately shed more light on the biophysical origins of these complexes.

CONCLUSIONS

In this study, we probed the molecular determinants of the interaction between two clinically relevant molecules, GMCSF and heparin. Combined SPR and solution NMR studies highlight pH-sensitive binding of heparin to GMCSF that is also dependent on the length of the heparin saccharide chain. These sensitivities in the GMCSF−heparin interaction impart subtle changes to the structural flexibility on GMCSF, which may optimize the protein scaffold and distort the terminal helix that exposes the His binding pocket.

ASSOCIATED CONTENT

Supporting Information

The Supporting Information is available free of charge at https://pubs.acs.org/doi/10.1021/acs.biochem.0c00538.

Raw SPR and NMR data, NMR line shape fitting, structure-based summaries of relaxation analyses, correlation plots depicting relaxation data, molecular docking of heparins onto GMCSF, evolution of RMSFs during MD simulations, and tables summarizing NMR relaxation data (PDF)

Accession Codes

Granulocyte macrophage colony stimulating factor (*Homo sapiens*), UniProtKB P04141. NMR resonance assignments for the acidic pH form of GMCSF were deposited into the BMRB as entry 50444.

AUTHOR INFORMATION

Corresponding Author

George P. Lisi − *Department of Molecular Biology, Cell Biology & Biochemistry, Brown University, Providence, Rhode Island 02903, United States;* orcid.org/0000-0001-8878-5655; Email: george_lisi@brown.edu

Authors

Jennifer Y. Cui − *Department of Molecular Biology, Cell Biology & Biochemistry, Brown University, Providence, Rhode Island 02903, United States;* orcid.org/0000-0002-1054-0786

Fuming Zhang − *Departments of Chemistry, Biology, and Chemical & Biological Engineering, Rensselaer Polytechnic Institute, Troy, New York 12180, United States;* orcid.org/0000-0003-2803-3704

Lukasz Nierzwicki − *Department of Bioengineering, University of California, Riverside, Riverside, California 92512, United States*

Giulia Palermo − *Department of Bioengineering, University of California, Riverside, Riverside, California 92512, United States;* orcid.org/0000-0003-1404-8737

Robert J. Linhardt − *Departments of Chemistry, Biology, and Chemical & Biological Engineering, Rensselaer Polytechnic Institute, Troy, New York 12180, United States;* orcid.org/0000-0003-2219-5833

Complete contact information is available at: https://pubs.acs.org/10.1021/acs.biochem.0c00538

Author Contributions

J.Y.C. expressed and purified GMCSF and collected and analyzed NMR and computational data. F.Z. and R.J.L. produced heparin oligos and collected and analyzed SPR data. L.N. and G.P. collected and analyzed MD simulation data. G.P.L. supervised the project and analyzed NMR data.

Funding

This work was supported by start-up funds from Brown University (to G.P.L.). G.P. acknowledges funding from the National Science Foundation under Grant CHE-1905374.

Notes

The authors declare no competing financial interest.

Plasmid DNA used in this work is freely available upon request. NMR pulse sequences used in this work were directly from the Bruker Pulse Program library. NMR processing scripts are freely available upon request.

ACKNOWLEDGMENTS

Computational resources for molecular dynamics simulations were provided by the COVID-19 HPC Consortium (https://covid19-hpc-consortium.org).

REFERENCES

(1) Shiomi, A., Usui, T., and Mimori, T. (2016) GM-CSF as a therapeutic target in autoimmune diseases. *Inflammation Regener. 36*, 8−17.

(2) van Nieuwenhuijze, A., Koenders, M., Roeleveld, D., Sleeman, M. A., van den Berg, W., and Wicks, I. P. (2013) GM-CSF as a therapeutic target in inflammatory diseases. *Mol. Immunol. 56*, 675−682.

(3) Mehta, H. M., Malandra, M., and Corey, S. J. (2015) G-CSF and GM-CSF in Neutropenia. *J. Immunol. 195*, 1341−1349.

(4) Huang, C., Wang, Y., Li, X., Ren, L., Zhao, J., Hu, Y., Zhang, L., Fan, G., Xu, J., Gu, X., Cheng, Z., Yu, T., Xia, J., Wei, Y., Wu, W., Xie, X., Yin, W., Li, H., Liu, M., Xiao, Y., Gao, H., Guo, L., Xie, J., Wang, G., Jiang, R., Gao, Z., Jin, Q., Wang, J., and Cao, B. (2020) Clinical features of patients infected with 2019 novel coronavirus in Wuhan, China. *Lancet 395*, 497−506.

(5) De Luca, G., Cavalli, G., Campochiaro, C., Della-Torre, E., Angelillo, P., Tomelleri, A., Boffini, N., Tentori, S., Mette, F., Farina,

N., Rovere-Querini, P., Ruggeri, A., D'Aliberti, T., Scarpellini, P., Landoni, G., De Cobelli, F., Paolini, J. F., Zangrillo, A., Tresoldi, M., Trapnell, B. C., Ciceri, F., and Dagna, L. (2020) GM-CSF blockade with mavrilimumab in severe COVID-19 pneumonia and systemic hyperinflammation: a single-centre, prospective cohort study. *The Lancet Rheumatology 2*, E465−E473.
(6) BioSpace (2020) Roivant doses first patient in pivotal BREATHE clinical trial evaluating gimsilumab in COVID-19 patients for the prevention and treatment of acute respiratory distress syndrome.
(7) Humanigen (2020) FDA approves initiation of Humanigen's phase III study of lenzilumab in COVID-19 patients.
(8) Kiniksa Pharmaceuticals (2020) Kiniksa reports data for mavrilimumab in COVID-19 pneumonia and hyperinflammation and for vixarelimab in diseases characterized by chronic pruritus.
(9) I-Mab Biopharma (2020) I-Mab announces IND clearance from FDA for TJM2 to treat cytokine release syndrome (CRS) associated with severe coronavirus disease 19 (COVID-19).
(10) Izana Bioscience (2020) Initiation of two-centre compassionate use study involving namilumab in the treatment of individual patients with rapidly worsening COVID-19 infection in Italy.
(11) Adams, B. (2020) GSK taps experimental arthritis antibody to calm the cytokine storm hitting COVID-19 patients. FierceBiotech.
(12) Lang, F. M., Lee, K. M., Teijaro, J. R., Becher, B., and Hamilton, J. A. (2020) GM-CSF-based treatments in COVID-19: reconciling opposing therapeutic approaches. *Nat. Rev. Immunol. 20*, 507−514.
(13) Liang, A., Du, Y., Wang, K., and Lin, B. (2006) Quantitative investigation of the interaction between granulocyte-macrophage colony-stimulating factor and heparin by capillary zone electrophoresis. *J. Sep. Sci. 29*, 1637−1641.
(14) Modrowski, D., Lomri, A., and Marie, P. J. (1998) Glycosaminoglycans bind granulocyte-macrophage colony-stimulating factor and modulate its mitogenic activity and signaling in human osteoblastic cells. *J. Cell. Physiol. 177*, 187−195.
(15) Sauve, S., Gingras, G., and Aubin, Y. (2008) NMR assignment of human granulocyte-macrophage colony-stimulating factor. *Biomol. NMR Assignments 2*, 5−7.
(16) Sebollela, A., Cagliari, T. C., Limaverde, G. S., Chapeaurouge, A., Sorgine, M. H., Coelho-Sampaio, T., Ramos, C. H., and Ferreira, S. T. (2005) Heparin-binding sites in granulocyte-macrophage colony-stimulating factor. Localization and regulation by histidine ionization. *J. Biol. Chem. 280*, 31949−31956.
(17) Wettreich, A., Sebollela, A., Carvalho, M. A., Azevedo, S. P., Borojevic, R., Ferreira, S. T., and Coelho-Sampaio, T. (1999) Acidic pH modulates the interaction between human granulocyte-macrophage colony-stimulating factor and glycosaminoglycans. *J. Biol. Chem. 274*, 31468−31475.
(18) Doukas, M., Chavan, A., Gass, C., Nickel, P., Boone, T., and Haley, B. (1995) Inhibition of Granulocyte-Macrophage Colony-stimulating Factor (GM-CSF) Activity by Suramin and Suramin Analogues Is Correlated to Interaction with the GM-CSF Nucleotide-binding Site. *J. Cancer Res. 55*, 5161−5163.
(19) Harter, K., Levine, M., and Henderson, S. O. (2015) Anticoagulation drug therapy: a review. *West J. Emerg. Med. 16*, 11−17.
(20) van der Meer, J. Y., Kellenbach, E., and van den Bos, L. J. (2017) From Farm to Pharma: An Overview of Industrial Heparin Manufacturing Methods. *Molecules 22*, 1025−1038.
(21) Warkentin, T. E., Sheppard, J. A., Horsewood, P., Simpson, P. J., Moore, J. C., and Kelton, J. G. (2000) Impact of the patient population on the risk for heparin-induced thrombocytopenia. *Blood 96*, 1703−1708.
(22) Avula, A., Nalleballe, K., Narula, N., Sapozhnikov, S., Dandu, V., Toom, S., Glaser, A., and Elsayegh, D. (2020) COVID-19 presenting as stroke. *Brain, Behav., Immun. 87*, 115−119.
(23) Oxley, T. J., Mocco, J., Majidi, S., Kellner, C. P., Shoirah, H., Singh, I. P., De Leacy, R. A., Shigematsu, T., Ladner, T. R., Yaeger, K. A., Skliut, M., Weinberger, J., Dangayach, N. S., Bederson, J. B., Tuhrim, S., and Fifi, J. T. (2020) Large-Vessel Stroke as a Presenting Feature of Covid-19 in the Young. *N. Engl. J. Med. 382*, e60.
(24) Yaghi, S., Ishida, K., Torres, J., Mac Grory, B., Raz, E., Humbert, K., Henninger, N., Trivedi, T., Lillemoe, K., Alam, S., Sanger, M., Kim, S., Scher, E., Dehkharghani, S., Wachs, M., Tanweer, O., Volpicelli, F., Bosworth, B., Lord, A., and Frontera, J. (2020) SARS-CoV-2 and Stroke in a New York Healthcare System. *Stroke 51*, 2002−2011.
(25) Schroeder, M. A., Lopez, S., Rettig, M. P., Trinkaus, K., Westervelt, P., and DiPersio, J. F. (2012) High Dose Sargramostim (GM-CSF) Combined with IV Plerixafor for the Mobilization of Peripheral Blood Stem Cells (PBSC) From Normal HLA-Matched Allogeneic Sibling Donors Results in Hypercoagulability. *Blood 120*, 4095−4095.
(26) Bonig, H., Burdach, S., Gobel, U., and Nurnberger, W. (2001) Growth factors and hemostasis: differential effects of GM-CSF and G-CSF on coagulation activation–laboratory and clinical evidence. *Ann. Hematol. 80*, 525−530.
(27) Aoki, H., Mogi, C., and Okajima, F. (2014) Ionotropic and metabotropic proton-sensing receptors involved in airway inflammation in allergic asthma. *Mediators Inflammation 2014*, 1−8.
(28) Huber, V., Camisaschi, C., Berzi, A., Ferro, S., Lugini, L., Triulzi, T., Tuccitto, A., Tagliabue, E., Castelli, C., and Rivoltini, L. (2017) Cancer acidity: An ultimate frontier of tumor immune escape and a novel target of immunomodulation. *Semin. Cancer Biol. 43*, 74−89.
(29) Ricciardolo, F. L., Gaston, B., and Hunt, J. (2004) Acid stress in the pathology of asthma. *J. Allergy Clin. Immunol. 113*, 610−619.
(30) Lee, W., Tonelli, M., and Markley, J. L. (2015) NMRFAM-SPARKY: enhanced software for biomolecular NMR spectroscopy. *Bioinformatics 31*, 1325−1327.
(31) Delaglio, F., Grzesiek, S., Vuister, G. W., Zhu, G., Pfeifer, J., and Bax, A. (1995) NMRPipe: a multidimensional spectral processing system based on UNIX pipes. *J. Biomol. NMR 6*, 277−293.
(32) Rozwarski, D. A., Diederichs, K., Hecht, R., Boone, T., and Karplus, P. A. (1996) Refined crystal structure and mutagenesis of human granulocyte-macrophage colony-stimulating factor. *Proteins: Struct., Funct., Genet. 26*, 304−313.
(33) Singh, A., Montgomery, D., Xue, X., Foley, B. L., and Woods, R. J. (2019) GAG Builder: a web-tool for modeling 3D structures of glycosaminoglycans. *Glycobiology 29*, 515−518.
(34) Abraham, M. J., Murtola, T., Schulz, R., Páll, S., Smith, J. C., Hess, B., and Lindahl, E. (2015) GROMACS: High performance molecular simulations through multi-level parallelism from laptops to supercomputers. *SoftwareX 1−2*, 19−25.
(35) Bonomi, M., Branduardi, D., Bussi, G., Camilloni, C., Provasi, D., Raiteri, P., Donadio, D., Marinelli, F., Pietrucci, F., Broglia, R. A., and Parrinello, M. (2009) PLUMED: A portable plugin for free-energy calculations with molecular dynamics. *Comput. Phys. Commun. 180*, 1961−1972.
(36) Yu, L., Li, D. W., and Bruschweiler, R. (2020) Balanced Amino-Acid-Specific Molecular Dynamics Force Field for the Realistic Simulation of Both Folded and Disordered Proteins. *J. Chem. Theory Comput. 16*, 1311−1318.
(37) Kirschner, K. N., Yongye, A. B., Tschampel, S. M., Gonzalez-Outeirino, J., Daniels, C. R., Foley, B. L., and Woods, R. J. (2008) GLYCAM06: a generalizable biomolecular force field. Carbohydrates. *J. Comput. Chem. 29*, 622−655.
(38) Bussi, G., Donadio, D., and Parrinello, M. (2007) Canonical sampling through velocity rescaling. *J. Chem. Phys. 126*, 014101.
(39) Parrinello, M., and Rahman, A. (1981) Polymorphic transitions in single crystals: A new molecular dynamics method. *J. Appl. Phys. 52*, 7182−7190.
(40) Darden, T. (1999) Ionic Charging Free Energies Using Ewald Summation. In *Rational Drug Design* (Truhlar, D., Blaney, J., and Dammkoehler, R. A., Eds.) pp 149−161, Springer, New York.
(41) Humphrey, W., Dalke, A., and Schulten, K. (1996) VMD: Visual molecular dynamics. *J. Mol. Graphics 14*, 33−38.

https://dx.doi.org/10.1021/acs.biochem.0c00538
Biochemistry 2020, 59, 3541−3553

(42) Hunter, J. D. (2007) Matplotlib: A 2D Graphics Environment. *Comput. Sci. Eng. 9*, 90−95.
(43) Kneller, J. M., Lu, M., and Bracken, C. (2002) An Effective Method for the Discrimination of Motional Anisotropy and Chemical Exchange. *J. Am. Chem. Soc. 124*, 1852−1853.
(44) Lisi, G. P., Manley, G. A., Hendrickson, H., Rivalta, I., Batista, V. S., and Loria, J. P. (2016) Dissecting Dynamic Allosteric Pathways using Chemically Related Small-Molecule Activators. *Structure 24*, 1155−1166.
(45) Lisi, G. P., East, K. W., Batista, V. S., and Loria, J. P. (2017) Altering the Allosteric Pathway in IGPS Suppresses Millisecond Motions and Catalytic Activity. *Proc. Natl. Acad. Sci. U. S. A. 114*, E3414−E3423.
(46) Lisi, G. P., and Loria, J. P. (2016) Solution NMR Spectroscopy for the Study of Enzyme Allostery. *Chem. Rev. 116*, 6323−6369.
(47) Kovrigin, E. L., Kempf, J. G., Grey, M. J., and Loria, J. P. (2006) Faithful Estimation of Dynamics Parameters from CPMG Relaxation Dispersion Measurements. *J. Magn. Reson. 180*, 93−104.
(48) Zega, A. (2017) NMR Methods for Identification of False Positives in Biochemical Screens. *J. Med. Chem. 60*, 9437−9447.
(49) Ciulli, A. (2013) Biophysical Screening for the Discovery of Small-molecule Ligands. *Methods Mol. Biol. 1008*, 357−388.
(50) Diwan, D., Shinkai, K., Tetsuka, T., Cao, B., Arai, H., Koyama, T., Hatano, K., and Matsuoka, K. (2017) Synthetic Assembly of Mannoe Moieties using Polymer Chemistry and the Biological Evaluation of its Interaction Towards Concanavalin A. *Molecules 22*, 157−168.

https://dx.doi.org/10.1021/acs.biochem.0c00538
Biochemistry 2020, 59, 3541−3553